Journal of Hydraulic Research

ISSN: 0022-1686 (Print) 1814-2079 (Online) Journal homepage: http://www.tandfonline.com/loi/tjhr20

A comprehensive two-phase flow model for unidirectional sheet-flows

Julien Chauchat

To cite this article: Julien Chauchat (2017): A comprehensive two-phase flow model for unidirectional sheet-flows, Journal of Hydraulic Research, DOI: 10.1080/00221686.2017.1289260

To link to this article: http://dx.doi.org/10.1080/00221686.2017.1289260

Published online: 02 May 2017.

IAHR AIRH
Taylor & Francis
Taylor & Francis Group

Journal of Hydraulic Research, 2017
https://doi.org/10.1080/00221686.2017.1289260

Research paper

A comprehensive two-phase flow model for unidirectional sheet-flows

JULIEN CHAUCHAT*, Associate Professor, *Laboratoire des Ecoulements Géophysiques et Industriels, UMR 5519, UJF, INPG, 1023 rue de de la piscine, 38400 Saint Martin d'Hères, France*
Email: julien.chauchat@grenoble-inp.fr

ABSTRACT
In this paper a comprehensive one-dimensional two-phase flow model for sediment transport under sheet-flow conditions is presented. The model is based on the dense granular flow rheology $\mu(\mathrm{I})$ for the intergranular stresses and on a mixing length model for the Reynolds shear stress. A drift velocity model is introduced to represent the vertical dispersion effects. Recent experimental data are used to improve the mixing length model and the numerical model is validated for four configurations. The model is further assessed by comparing the dependence of the sediment transport rate and the sheet layer thickness on the Shields number. The good agreement with experimental data confirms the capability of the model formulation to reproduce unidirectional sheet-flows. The agreement with the latest kinetic theory of granular flows based model demonstrate that the dense granular flow rheology can be used as an alternative approach to kinetic theory in two-phase flow models.

Keywords: Bedload; benthic boundary layers and near-bed processes; eddy-viscosity closures; particle-laden flows; suspended sediments; turbulence-sediments interactions

1 Introduction

The sheet-flow regime of sediment transport occurs when the fluid flow is strong enough to mobilize a thick and dense layer of particles on the top of the sediment bed. Provided that the particles are light enough or the shearing is strong enough, sediment particles can be entrained in suspension to form a suspension layer above the sheet layer. It is widely accepted that both intergranular interactions and turbulent processes are key mechanisms in momentum diffusion and dilatancy effects (e.g. Bagnold, 1956; Jenkins & Hanes, 1998). In this paper, we focus on uniform and steady sheet-flows of well-sorted particles in which the slope is sufficiently low to neglect the body force acting on the particles.

Two dimensionless numbers, the Shields number θ and the suspension number S, are considered to characterize this transport mode. The Shields number is the ratio between the force exerted by the fluid on a single particle and its apparent weight $\theta = \rho_f u_*^2/(\rho_s - \rho_f)(g d_p)$ where ρ_f and ρ_s are the fluid and sediment densities, u_* is the bed friction velocity, g is the gravity acceleration and d_p the particle diameter. In the literature, the transition from the bedform regime to the sheet-flow one is shown to occur for a Shields number around 0.5. Above this value, the sheet-flow layer thickness (δ_s) and the associated solid load (q_s) are dependent on the Shields number (e.g. Einstein, 1950; Wilson, 1966; Yalin, 1977). Second, the suspension number $\mathsf{S} = w/u_*$ characterizes the competition between particle inertia, represented by the settling velocity (w) and the turbulent velocity fluctuation magnitude, represented by the bed friction velocity (u_*). The suspension number can be seen as a macroscopic Stokes number. Following (Sumer, Kozakiewicz, Fredsoe, & Deigaard, 1996), when $w/u_* < 0.8$ the suspended-load dominates the bed-load in the so-called suspension mode. By contrast, when $w/u_* > 1$, the bed-load dominates the suspended-load in the so-called no-suspension mode.

First attempts in modelling sheet-flows have been made by Hanes and Bowen (1985) and Wilson (1987). In these models the concentration profile is prescribed and the intergranular stresses are given by an empirical law (e.g. Bagnold, 1954). Over the past 15 years, two-phase models based on the kinetic theory of granular flows to describe intergranular stresses have been applied with some success to model the sheet-flow regime (e.g. Hsu, Jenkins, & Liu, 2004; Jenkins & Hanes, 1998). In these models, the kinetic theory has been stated for situations in which collisional interactions are the dominant mechanisms of momentum transfer. The concentration profile is obtained from a balance between collisional interactions and gravity as a result

Received 21 November 2015; accepted 21 January 2017/Currently open for discussion.

∗ Current affiliation: ENSE3, Université Grenoble Alpes, LEGI, G-INP, CNRS, F-38000 Grenoble, France

ISSN 0022-1686 print/ISSN 1814-2079 online
http://www.tandfonline.com

of the model. More recently, Berzi (2011) and Berzi and Fraccarollo (2013) developed analytical solutions for sheet flows based on the kinetic theory. In the latest version they incorporated a mixing length and a granular like contribution to the fluid stress (Berzi & Fraccarollo, 2015) as well as a turbulent suspension layer accounting for the suspended load (Berzi & Fraccarollo, 2016). Based on these analytical solutions the authors have been able to draw phase diagrams for sediment transport, allowing differentiation between sheet flows and debris flows, and between ordinary bed-load, collisional sediment transport, with and without suspension, and fully turbulent suspension as a function of the Shields number, particulate Reynolds number and bed slope (Berzi & Fraccarollo, 2013, 2016).

Over the past decade the dense granular flow rheology $\mu(\mathrm{I})$ (GDRmidi, 2004) has been proposed to describe intergranular stresses in dry granular flows. This phenomenological approach has been used in two-phase flow sediment transport models (e.g. Chiodi, Claudin, & Andreotti, 2014; Ouriemi, Aussillous, & Gauzzelli, 2009; Revil-Baudard & Chauchat, 2013) and comparison with experiments has shown the potential of this rheology to capture the main features of sediment transport. It represents an alternative approach to kinetic theory. The dense granular flow rheology is based on the dimensional analysis of the simple shear configuration (Forterre & Pouliquen, 2008), the shear to normal stress ratio, denoted as μ, and the solid phase volume fraction ϕ are function of a dimensionless number I. Depending on the role of the interstitial fluid Courrech du Pont, Gondret, Perrin, and Rabaud (2003) and Cassar, Nicolas, and Pouliquen (2005) introduced three different granular flow regimes: free-fall, viscous and turbulent regimes. For each one, the formulation of the dimensionless number I is different. Boyer, Guazzelli, and Pouliquen (2011) have thoroughly investigated the viscous regime using annular shear cell experiments. Aussillous, Chauchat, Pailha, Médale, and Guazzelli (2013) have used the formulation of Boyer et al. (2011) to reproduce laminar bed-load experiments. In this situation, the volume fraction of particles is almost constant throughout the moving layer and the $\phi(\mathrm{I})$ relationship is not required in the model. Revil-Baudard and Chauchat (2013) have shown that for turbulent sheet flows the dense granular flow regime is in the free-fall one for the no-suspension mode ($w/u_* > 1$) and in the turbulent regime for the suspension mode ($w/u_* < 1$). In both cases, the $\phi(\mathrm{I})$ relationship is able to qualitatively reproduce the decrease of sediment concentration in the moving sediment layer. Chiodi et al. (2014) have proposed an improved two-phase flow model valid in the viscous and turbulent flow regimes. The proposed model is able to reproduce the scaling law proposed by Meyer-Peter and Muller (1948) for the solid flux versus the Shields number as well as the exchange of mass between the suspension and the bed-load layer without any empirical parametrization. According to the authors' conclusion, this model still needs to be compared with experimental or numerical data.

Concerning laboratory experiments on sheet-flows, the first small scale laboratory experiments designed to study the vertical structure of uniform and steady sheet-flows were conducted in pipe flows by Daniel (1965), Wilson (1966), Nnadi and Wilson (1992) and Pugh and Wilson (1999). Mean local volumetric concentration (ϕ) and fluid streamwise velocities (u) were measured using γ-ray technique and a conductivity probe, respectively. However, velocity and concentration have never been measured during the same experiment. Sumer et al. (1996) have performed free surface and duct flow experiments using capacity probes for concentration and a Pitot device for streamwise velocity measurements. Again, no dataset exists with both velocity and concentration for the same run. Matoušek (2009) did sheet flow experiments and measured concentration profiles using a gamma-ray technique and averaged quantities for the fluid and solid discharges. Spinewine, Capart, Fraccarollo, and Larcher (2011) and Capart and Fraccarollo (2011) have used video techniques to get both streamwise velocity and concentration profiles at the side-wall. This dataset is more complete but the measurements are available for the particles only and are not collocated between velocity and concentration. Also, no information on the fluid flow profile is available. More recently, Revil-Baudard, Chauchat, Hurther, and Barraud (2015) have presented a new experimental dataset obtained using the Acoustic Velocity and Concentration Profiler (ACVP) (Hurther, Thorne, Bricault, Lemmin, & Barnoud, 2011) to measure collocated two-component velocities and concentration measurements over the entire water column at the centreline of the channel. This new dataset allows investigation of turbulence closures for the momentum and sediment diffusivities.

The purpose of the present contribution is to extend the model by Revil-Baudard and Chauchat (2013) to develop a single layer model solving the two-phase equations over the entire domain and to use the new experimental data presented in Revil-Baudard et al. (2015) to improve the constitutive laws. The two-phase flow model is presented in Section 2. Improved constitutive laws are proposed and used to validate the model on two experimental datasets in Section 3. The predicted sediment transport rate and sheet layer thickness for a wide range of Shields numbers are further compared with experimental data and models from the literature. In Section 4, the main conclusions of the paper are given and guidelines for future research are drawn.

2 Two-phase flow model formulation

The proposed model is inspired from previous works (Revil-Baudard & Chauchat, 2013; Chauchat, Guillou, Bang, & Nguyen, 2013). It is based on the two-phase equations of Jackson (2000) that consists in mass and momentum balance equations for both fluid and solid phases:

$$\frac{\partial \epsilon \rho_f}{\partial t} + \nabla \cdot (\epsilon \rho_f \boldsymbol{u}_f) = 0; \quad \frac{\partial \phi \rho_s}{\partial t} + \nabla \cdot (\phi \rho_s \boldsymbol{u}_s) = 0 \tag{1}$$

$$\frac{\partial \epsilon \rho_f \boldsymbol{u_f}}{\partial t} + \nabla \cdot (\epsilon \rho_f \boldsymbol{u_f} \otimes \boldsymbol{u_f}) = -\nabla p_f + \epsilon \rho_f \boldsymbol{g} + \epsilon \nabla \cdot \boldsymbol{\tau}^f + \nabla \cdot \mathbf{R_f} - n\boldsymbol{f_D} \quad (2)$$

$$\frac{\partial \phi \rho_s \boldsymbol{u_s}}{\partial t} + \nabla \cdot (\phi \rho_s \boldsymbol{u_s} \otimes \boldsymbol{u_s}) = -\nabla p_s - \phi \nabla p_f + \phi \rho_s \boldsymbol{g} + \phi \nabla \cdot \boldsymbol{\tau}^f + \nabla \cdot \boldsymbol{\tau}^s + n\boldsymbol{f_D} \quad (3)$$

where ϵ and ϕ are the volume fraction of fluid and solid phase respectively, ρ_k and $\boldsymbol{u}_k$ are the density and the velocity vector of phase k, p_k and $\boldsymbol{\tau}^k$ are the pressure and shear stress tensor associated with phase k, $\mathbf{R_f}$ is the fluid Reynolds stress tensor, $\boldsymbol{g}$ is the gravity acceleration vector, $\boldsymbol{f_D}$ represents the drag force exerted by the fluid on a single particle and n is the number of particles per unit volume. Phase k stands for either f for the fluid phase or s for the solid phase. In addition to these conservation equations, the overall volume conservation imposes that:

$$\phi + \epsilon = 1 \quad (4)$$

2.1 *One-dimensional formulation*

In this work we focus on uniform flow conditions, therefore the only velocity components that do not vanish are u and w and they only depend on the vertical position z. With these assumptions, the mass conservation equations for each phase reduces to:

$$\frac{\partial \epsilon \rho_f}{\partial t} + \frac{\partial \epsilon \rho_f w_f}{\partial z} = 0; \quad \frac{\partial \phi \rho_s}{\partial t} + \frac{\partial \phi \rho_s w_s}{\partial z} = 0 \quad (5)$$

The direction z is normal to the channel bottom and upward oriented. The mass conservation for the mixture reads:

$$\frac{\partial}{\partial z}(\phi w_s + \epsilon w_f) = 0 \quad (6)$$

meaning that the mixture is incompressible. Equation (4) still holds: $\epsilon = 1 - \phi$.

With these assumptions the momentum equations for both phases and for the streamwise (Ox) and wall-normal (Oz) directions simplify as follow:

$$\frac{\partial \epsilon \rho_f u_f}{\partial t} + w_f \frac{\partial \epsilon \rho_f u_f}{\partial z} = \epsilon \rho_f g \sin(\beta) + \epsilon \frac{\partial \tau^f_{xz}}{\partial z} + \frac{\partial R^f_{xz}}{\partial z} - n f_{Dx} \quad (7)$$

$$\frac{\partial \phi \rho_s u_s}{\partial t} + w_s \frac{\partial \phi \rho_s u_s}{\partial z} = \phi \rho_s g \sin(\beta) + \phi \frac{\partial \tau^f_{xz}}{\partial z} + \frac{\partial \tau^s_{xz}}{\partial z} + n f_{Dx} \quad (8)$$

$$\frac{\partial \epsilon \rho_f w_f}{\partial t} + w_f \frac{\partial \epsilon \rho_f w_f}{\partial z} = -\epsilon \frac{\partial p_f}{\partial z} - \epsilon \rho_f g \cos(\beta) + \epsilon \frac{\partial \tau^f_{zz}}{\partial z} - n f_{Dz} \quad (9)$$

$$\frac{\partial \phi \rho_s w_s}{\partial t} + w_s \frac{\partial \phi \rho_s w_s}{\partial z} = -\frac{\partial p_s}{\partial z} - \phi \frac{\partial p_f}{\partial z} - \phi \rho_s g \cos(\beta) + \phi \frac{\partial \tau^f_{zz}}{\partial z} + n f_{Dz} \quad (10)$$

In the present contribution we attempt to provide a consistent numerical model with adequate closure laws for application to sediment transport in the sheet-flow regime. The terms that need closures are the viscous shear stress τ^f_{xz}, the fluid Reynolds shear stress R^f_{xz}, the particulate shear stress τ^s_{xz}, the particulate pressure p_s and the drag force nf_{Dx} and nf_{Dz}.

2.2 *Closures*

The closures are inspired from Revil-Baudard and Chauchat (2013) in which the viscous shear stress is based on an effective viscosity depending on the solid phase volume fraction, the turbulent Reynolds shear stress is based on a mixing length formulation, the particulate shear stress and the particulate pressure are based on the dense granular flow rheology. The drag force is based on an empirical correlation for the drag coefficient and the turbulent dispersion effects are included based on the drift velocity concept as in Chauchat and Guillou (2008).

Viscous and Reynolds shear stresses

As proposed by Jackson (1997, 2000) the effective viscous shear stress is proportional to the shear rate of the mixture with an effective viscosity η_{mix} that depends on the particulate phase volume fraction:

$$\tau^f_{xz} = \eta_{mix} \frac{\mathrm{d}U}{\mathrm{d}z} \quad (11)$$

where $U = \epsilon u_f + \phi u_s$ is the volume averaged mixture velocity. The model proposed by Boyer et al. (2011) is used for the mixture viscosity:

$$\frac{\eta_{mix}}{\eta_f} = 1 + 2.5\phi \left(1 - \frac{\phi}{\phi^{\max}}\right)^{-1} \quad (12)$$

It should be pointed out that, due to the incompressibility of the mixture, the effective viscous stress cancels out in the vertical momentum equation.

The Reynolds shear stress is modelled using a simple mixing length approach in which the mixing length is parameterized based on the integral of the particulate phase volume fraction against the vertical direction:

$$R^f_{xz} = \eta_t \frac{\mathrm{d}U}{\mathrm{d}z} \quad (13)$$

where $\eta_t = \epsilon \rho_f l_m^2 |\mathrm{d}U/\mathrm{d}z|$ and

$$l_m = \kappa \int_0^z 1 - \left(\frac{\phi(\xi)}{\phi^{\max}}\right)^{n_{lm}} \mathrm{d}\xi \quad (14)$$

where κ is the von Karman constant and n_{lm} is an empirical exponent that will be discussed in Section 3. The case $n_{lm} = 1$ has been proposed by Li and Sawamoto (1995) and used by Dong and Zhang (1999) and Revil-Baudard and Chauchat (2013) to model sheet-flows.

Particulate shear stress

The particulate shear stress is based on the dense granular flow rheology (Forterre & Pouliquen, 2008):

$$\tau_{xz}^s = \mu(\mathsf{I})p_s \tag{15}$$

in which the friction coefficient μ depends on the inertial number $\mathsf{I} = |\mathrm{d}u_s/\mathrm{d}z|d_p\sqrt{\rho_s/p_s}$ and is defined as:

$$\mu(\mathsf{I}) = \mu_s + \frac{\mu_2 - \mu_s}{\mathsf{I}_0/\mathsf{I} + 1}$$

In the relationship above, d_p is the particle diameter, μ_s is the static friction coefficient, μ_2 is an empirical dynamical coefficient and I_0 is an empirical constant of the rheology. For glass beads in air the typical values are: $\mu_s = 0.38$, $\mu_2 = 0.64$ and $\mathsf{I}_0 = 0.3$ (Jop, Forterre, & Pouliquen, 2006).

A solid phase viscosity can be written by identifying Eq. (15) with $\tau_{xz}^s = \eta_s|\mathrm{d}u_s/\mathrm{d}z|$ leading to $\eta_s = \mu(\mathsf{I})p_s/|\mathrm{d}u_s/\mathrm{d}z|$. This mathematical expression is not defined if the shear rate vanishes $|\mathrm{d}u_s/\mathrm{d}z| = 0$. The regularization proposed by Chauchat and Médale (2014) is adopted:

$$\eta_s = \frac{\mu(\mathsf{I})\, p_s}{\left(\left|\dfrac{\mathrm{d}u_s}{\mathrm{d}z}\right|^2 + \lambda^2\right)^{1/2}} \tag{16}$$

where λ is the regularization parameter. It is fixed to $\lambda = 10^{-6}\mathrm{s}^{-1}$ for all the simulations presented herein.

Particle pressure

The particulate pressure represents the resistance to compression of the solid phase. In the present problem two different contributions have to be considered: one originates from the permanent contact between the particles and the other one originates from the shearing of the granular media. Following Johnson and Jackson (1987) the total particulate pressure is obtained as the sum of these two contributions: $p_s = p_s^c + p_s^s$, where p_s^c is related to permanent contact and p_s^s is related to shear induced mechanisms (frictional/collisional interactions).

The permanent contact contribution to the particulate pressure can be written following Johnson and Jackson (1987) as:

$$p_s^c = \Pi_0(\phi^{\max} - \phi)^{-\zeta} \tag{17}$$

where Π_0 and ζ are two empirical parameters. In the present paper we have used the following values: $\Pi_0 = 4 \times 10^{-35}$ Pa and $\zeta = 15$. When using the frictional rheology $\mu(\mathsf{I})$ it is critical that the hydrostatic particulate pressure is recovered in the static bed as the particulate viscosity is proportional to the particulate pressure.

Concerning the shear induced contribution, it can be obtained from the dilatancy law $\phi(\mathsf{I})$ as proposed by Boyer et al. (2011) for the viscous regime of the granular flow rheology. The adaptation to the inertial regime leads to:

$$\phi(\mathsf{I}) = \frac{\phi^{\max}}{1 + b\mathsf{I}} \tag{18}$$

Developing this expression in a Taylor expansion around $\mathsf{I} = 0$ and identifying with the linear relationship proposed in Forterre and Pouliquen (2008) the coefficient b must be equal to one-third ($b = 1/3$). Inverting Eq. (18) and substituting the definition of the inertial number I gives the following expression for the shear induced pressure:

$$p_s^s = \left(\frac{b\phi}{\phi^{\max} - \phi}\right)^2 \rho_s d_p \left|\frac{\mathrm{d}u_s}{\mathrm{d}z}\right|^2 \tag{19}$$

Drag force

The drag force is modelled following Chauchat and Guillou (2008) as:

$$n\boldsymbol{f}_D = \frac{\phi\rho_s}{\tau_{fs}}(\boldsymbol{u_r} + \boldsymbol{u_d}) \tag{20}$$

where $\boldsymbol{u_r} = \boldsymbol{u_f} - \boldsymbol{u_s}$ is the relative velocity, $\boldsymbol{u_d}$ is the drift velocity and τ_{fs} is the particle relaxation time defined as:

$$\tau_{fs} = \left(\frac{3\rho_f}{4\rho_s\tilde{d}_p}C_D\|\boldsymbol{u_r} + \boldsymbol{u_d}\|\epsilon^{2-n_{RZ}}\right)^{-1} \tag{21}$$

where C_D is the averaged drag coefficient for a single particle (Schiller & Naumann, 1933): $C_D = (24/\mathsf{R_p})(1 + 0.15\mathsf{R_p}^{0.687})$ where $\mathsf{R_p} = \| \boldsymbol{u_r} \| \tilde{d}_p/\nu_f$ is the particulate Reynolds number in which $\| \boldsymbol{u_r} \| = \sqrt{(u_f - u_s)^2 + (w_f - w_s)^2}$. A shape factor ψ has been introduced: $\tilde{d}_p = \psi d_p$, to account for the influence of non-sphericity of the particles on the settling velocity. The term $\epsilon^{2-n_{RZ}}$ is the hindrance function proposed by Richardson and Zaki (1954), where $n_{RZ} = 3.65$ is an empirical coefficient, that accounts for the decrease of the particle settling velocity when the local concentration of particles increases.

The drift velocity $\boldsymbol{u_d}$, of components u_d and w_d, represents the fluid velocity fluctuations "seen by the particles" (Simonin & Viollet, 1990), also sometimes called the turbulent slip velocity. More generally, it represents the dispersion effects on the particle phase induced by the turbulent velocity fluctuations. In this paper, only the vertical component is modelled:

$$w_d = -\frac{\eta_t}{\rho_f\,\sigma_s\phi}\frac{\mathrm{d}\phi}{\mathrm{d}z} \tag{22}$$

where σ_s is the turbulent Schmidt number, the ratio of the eddy viscosity to the sediment turbulent diffusivity. This formulation ensures that the two-phase flow model is fully consistent with the Rouse profile; the interested reader is referred to Appendix 1 for a complete demonstration.

The drift velocity component in the streamwise direction u_d would represent the existence of a lag velocity (Bouvard & Petkovic, 1985; Muste & Patel, 1997). Due to the lack of experimental data for this quantity under sheet flow conditions this term is neglected in the present model.

The governing equations are discretized using a finite volume technique for the mass conservation equation and a finite difference technique for the momentum balance. A staggered grid is used with the velocities located at the cell face and the scalar quantities, such as volume fraction or viscosities, located at the cell centre. For the pressure velocity coupling a projection method (Chorin, 1968; Temam, 1969) is used. The numerical schemes are Euler implicit for the time derivative, upwind for the advection terms and central difference for the diffusion terms. For additional information on the numerical model, the reader is referred to Chauchat et al. (2013).

Even if the problem is steady the choice of a transient solver is made to allow for future applications of the model to unsteady situations such as flood, tides or waves, and to prepare the development of a multi-dimensional numerical model for which a pressure-velocity algorithm is the corner stone.

3 Results and discussion

In this section, the two-phase flow model presented above is applied to uniform and unidirectional sheet-flows. First, the mixing length parameters are adjusted based on experimental measurements reported in Revil-Baudard et al. (2015). Second, the numerical model is validated against two experimental datasets: Revil-Baudard et al. (2015) and Sumer et al. (1996). The range of Shields numbers investigated is between 0.44 and 2.1 and the range of suspension numbers varies between 0.84 to 1.1, which corresponds to the transition between suspension and no-suspension sheet-flow regimes (Sumer et al., 1996). Additional numerical simulations have been performed to extend the range of Shields numbers up to 3.3 and the numerical results are compared with experimental data and model predictions for the dependence of the dimensionless sediment transport rate and the sheet layer thickness on the Shields number.

The experiments reported in Revil-Baudard et al. (2015) were performed in a tilting flume 10 m long and 0.35 m wide with a bed slope of $\beta = 0.005$. The sediments are irregularly shaped (PMMA, density $\rho_s = 1192\,\mathrm{kg\,m^{-3}}$), with a tangent of the angle of repose measured at $\mu_s^m = 0.7$. The grain size distribution is quite well-sorted and centred around $d_p = 3\,\mathrm{mm} \pm 0.5\,\mathrm{mm}$. The mean settling velocity is equal to $w = 5.59\,\mathrm{cm\,s^{-1}}$, which was determined experimentally from settling tests in a still water tank (see Table 1).

Figure 1a shows the velocity and concentration profiles made dimensionless by their respective maximum values as obtained in the experiments (Revil-Baudard et al., 2015). In Fig. 1b, the experimental Schmidt number σ_s profile is plotted; it exhibits a constant value of $\sigma_s = 0.44$ for $z/d_p > 5$. This value will be used for the vertical component of the drift velocity in Eq. (22). The measured value is consistent with the parametrization from Van Rijn (1984): $\sigma_s = (1 + 2(w/u_*)^2)^{-1}$ that leads to a Schmidt number of 0.3 in this configuration.

Figure 1c shows the experimental mixing length profile together with the best fit presented in Revil-Baudard et al. (2015): $l_m = \kappa(z - z_d)$ with $\kappa = 0.225$ and $z_d = 3.1\ d_p$. These results show that the von Karman constant is drastically reduced under sheet-flow conditions and that the zero plane bed (z_d) is vertically shifted upward compared with the $u_f = 0$ plane. This is an issue for using mixing length under sheet-flow conditions as this value has to be parameterized. The mixing length proposed in Eq. (14) allows us to circumvent the issue of imposing the zero plane bed position, i.e. the mixing length origin. It is a purely empirical formulation that is for the first time compared with detailed measurements in a turbulent boundary layer above a mobile bed. The profile obtained by using Eq. (14) with $n_{lm} = 1$ and a von Karman constant of $\kappa = 0.225$ is shown by the green dashed dotted line. The agreement is satisfactory but the mixing length is slightly underestimated. The red dashed line corresponds to the solution of Eq. (14) with $n_{lm} = 1.66$ and a von Karman constant of $\kappa = 0.225$. The agreement is much better for $z/d_p > 5$. The influence of this parametrization will be discussed in the following text. Recently, Berzi and Fraccarollo (2015) proposed a parametrization of the mixing length for collisional suspension based only on the local concentration:

$$\frac{l_m}{d_p} = 3(\phi^{\max} - \phi)^3 \tag{23}$$

This parametrization is presented in Fig. 1c as the magenta dotted line. The behaviour of this mixing length in the region of

Table 1 Physical parameters for the numerical simulations

Case	S_f	h (m)	z_{int} (m)	ϕ^0 (–)	$\phi^{\max}$ (–)	d_p (mm)	ρ_p/ρ_f (–)	w ($\mathrm{ms^{-1}}$)	μ_s^m (–)	θ (–)	$\mathrm{S} = w/u_*$ (–)
RB	0.0019	0.2	0.0541	0.53	0.55	3	1.19	0.0559	0.7	0.44	1.1
SUM A	0.0079	0.104	0.0526	0.5	0.6	2.6	1.14	0.073	0.51	1.38	1.04
SUM B	0.0091	0.104	0.0521	0.5	0.6	2.6	1.14	0.073	0.51	1.63	0.95
SUM C	0.0105	0.104	0.0516	0.5	0.6	2.6	1.14	0.073	0.51	2.18	0.84

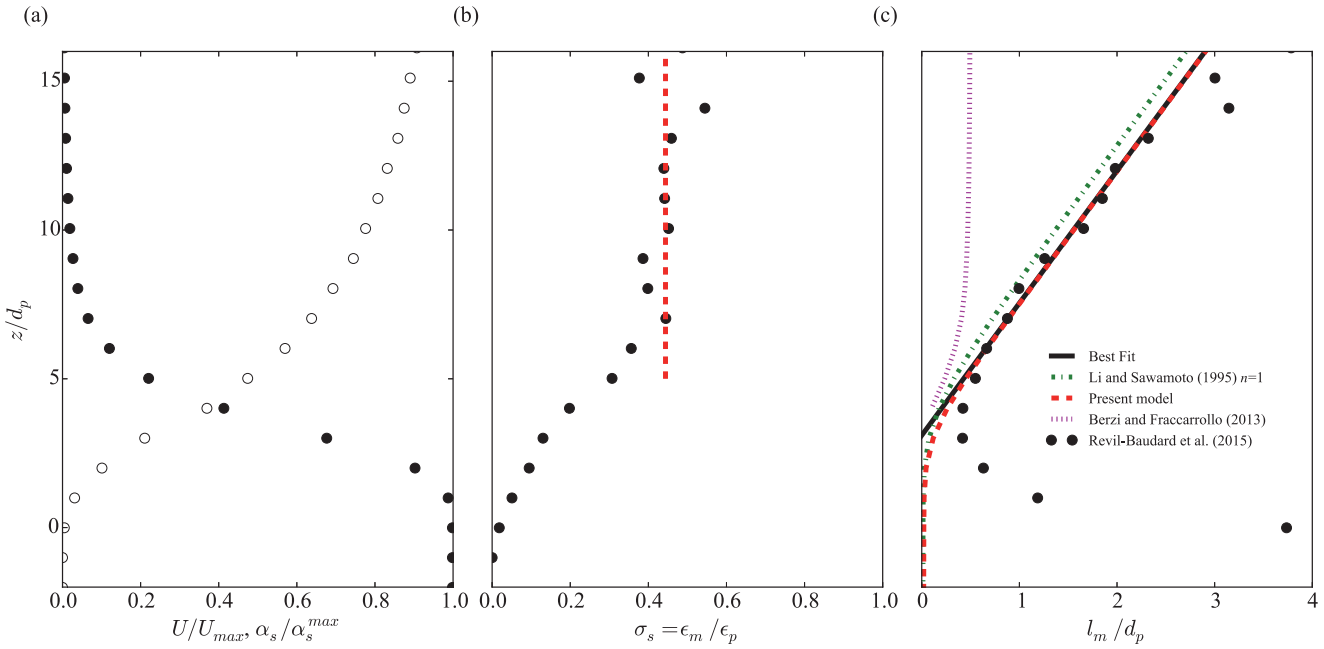

Figure 1 Dimensionless experimental mean velocity and mean concentration profiles: (a) dimensionless experimental mean velocity ○ and mean concentration profiles ● ; (b) the experimental Schmidt number profile; and (c) the mixing length profiles

intermediate concentration ($0.3 > \phi > 0.1$) is good even if a better agreement could be obtained by adjusting the parameters of this empirical law. However, the mixing length of Berzi and Fraccarollo (2015) cannot reproduce the linear behaviour in the dilute suspension layer as measured in Revil-Baudard et al. (2015). This model is probably only valid in the collisional layer. Obviously, it can not reproduce the logarithmic layer characteristic of turbulent boundary layers. It is possible that the small submergence, i.e. a small water depth to particle diameter ratio in the Capart and Fraccarollo (2011) experiments used to derive this model, can explain this limitation.

The model presented in Section 2 is used together with the constitutive laws proposed above to perform a comparison with experimental data presented in Revil-Baudard et al. (2015) and Sumer et al. (1996). The numerical model has been run using Nz grid points uniformly distributed (see Table 2) and an initial condition at rest ($u_f = w_f = u_s = w_f = 0$); the particulate phase volume fraction profile is set according to a hyperbolic tangent profile: $\phi = \phi^0\ 1/2\left\{1 + \tanh\left[200\ \left(z_{int}(\phi^{\max}/\phi^0) - z\right)\right]\right\}$, where z_{int} corresponds to the initial "bed interface" elevation, ϕ^0 is the initial solid volume fraction and z is the vertical coordinate. The runs are performed using the measured friction slope S_f and the measured water depth for the Revil-Baudard et al. (2015) experiment. For the experiments of Sumer et al. (1996), in order to avoid solving for the boundary layer at the top rigid lid, the experimentally estimated hydraulic radius has been preferred. The initial interface position is chosen to reach approximately the same Shields parameter than in the experiments at steady state. The complete set of boundary conditions are presented in Table 3.

Two numerical simulations have been performed to evaluate the influence of the mixing length parametrization (Eq. (14)): RB1 ($n_{lm} = 1$) and RB2 ($n_{lm} = 1.66$). The granular rheology parameters have been chosen according to the values for glass beads in air, the μ_s value is identical to the measured value of the tangent of the angle repose (μ_s^m), the difference $\mu_2 - \mu_s = 0.26$, $\mathrm{I}_0 = 0.3$ and $b = 1/3$. The resulting mean velocity, mean concentration and Reynolds shear stress profiles are shown in Fig. 2. The run RB1 with exponent $n_{lm} = 1$ leads to an overestimated fluid velocity in the outer region ($\approx$ 20%). The results obtained in run RB2 are in better agreement with the measurements. The concentration profile is well predicted in the suspension layer but the agreement is not as good in the more concentrated region of the flow ($\phi > 0.25$), suggesting that the granular rheology has

Table 2 Model parameters for the different runs

Run name	Configuration	κ	n_{lm}	σ_s	μ_s	μ_2	I_0	b	ψ	Nz
RB1	Revil-Baudard et al. (2015)	0.225	1	0.44	0.7	0.96	0.3	1/3	0.5	401
RB2	Revil-Baudard et al. (2015)	0.225	1.66	0.44	0.7	0.96	0.3	1/3	0.5	401
RB3	Revil-Baudard et al. (2015)	0.225	1.66	0.44	0.52	0.96	0.6	2/3	0.5	401
SUM A1/B1/C1	Sumer et al. (1996)	0.225	1.66	0.44	0.51	0.77	0.3	1/3	0.945	201
SUM A2/B2/C2	Sumer et al. (1996)	0.225	1.66	0.44	0.38	0.82	0.6	2/3	0.945	201

Table 3 Boundary conditions

BC	ϕ	u_f	w_f	u_s	w_s	p
Bottom	$\frac{\partial \phi}{\partial z} = 0$	$u_f = 0$	$w_f = 0$	$u_s = 0$	$w_s = 0$	$\frac{\partial p}{\partial z} = 0$
Top	$\frac{\partial \phi}{\partial z} = 0$	$\frac{\partial u_f}{\partial z} = 0$	$\frac{\partial w_f}{\partial z} = 0$	$\frac{\partial u_s}{\partial z} = 0$	$\frac{\partial w_s}{\partial z} = 0$	$p = 0$

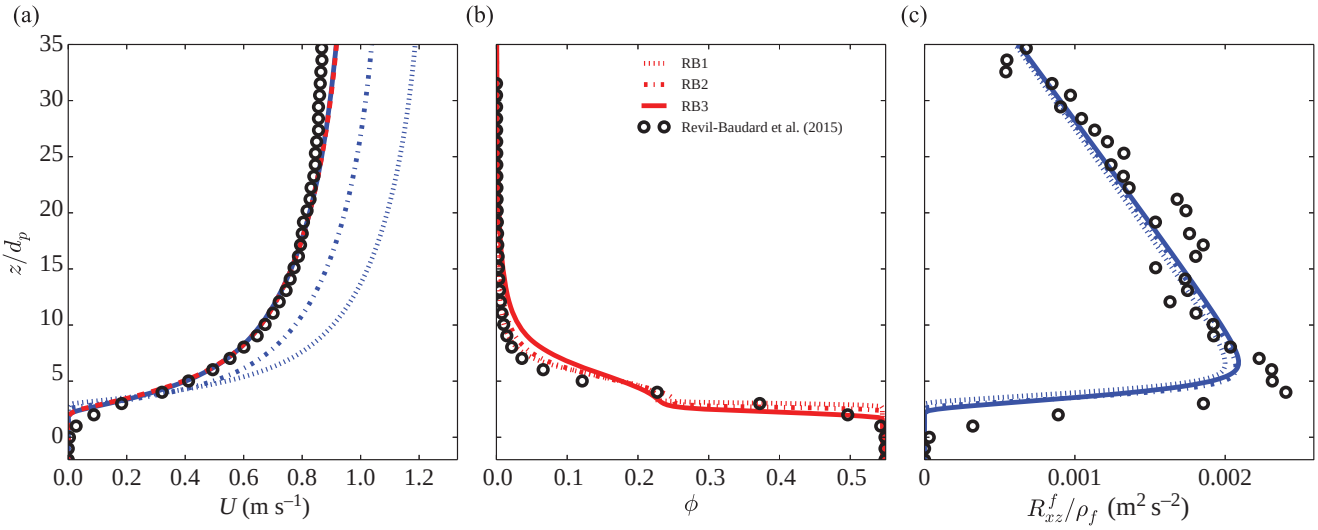

Figure 2 Comparison of numerical results for case RB1, RB2 and RB3 with experimental data. (a) Fluid and particulate phase velocity profiles for case RB1 (u_f : blue dotted line), RB2 (u_f : blue dashed-dotted line) and RB3 (u_f : blue solid line; u_s: red dashed line). (b) Concentration profile for case RB1 (red dotted line), RB2 (red dashed-dotted line) and RB3 (red solid line). (c) Reynolds shear stress profile for case RB1 (blue dotted line), RB2 (blue dashed-dotted line) and RB3 (blue solid line). The symbols represent experimental data from Revil-Baudard et al. (2015)

to be modified. The predicted shear stress profile (panel c) nicely coincides with the experimental one meaning that the friction slope and the water depth used in the simulation are consistent with the experimental conditions. The Shields number is equal to $\theta = 0.45$, obtained by extrapolating the shear stress profile to $z = 0$ corresponding to the $u_f = 0$ plane.

For confirmation, the two-phase flow model is run on Sumer et al. (1996) configurations; the physical parameters are synthesized in Table 1. Three cases, for which velocity profile measurements are available, have been run corresponding to Shields numbers $\theta = 1.38$ (SUM A), $\theta = 1.63$ (SUM B) and $\theta = 2.18$ (SUM C). Figure 3 shows the comparison of the two-phase flow model results with experimental fluid velocity profiles in panel (a). Run SUMA1/B1/C1 corresponds to granular rheology parameters for glass beads (see Table 2). The concentration profile (panel b) and shear stress profile (panel c) are given for reference but no experimental data are available for these configurations. Using glass bead parameters for the granular flow rheology leads to overestimated fluid velocity in the upper part of the profile and too strong velocity gradient in the lower part of the profile compared with measurements for the three cases SUMA1/B1/C1 (see left panel of Fig. 3). The concentration profiles exhibit a concentration shoulder as reported in Revil-Baudard and Chauchat (2013).

The rheological parameters of the sheet flow model have been optimized over the four configurations (RB, SUMA/B/C) using trial and error. The following values have been retained: μ_s is reduced by 25% compared with the tangent of the angle of repose μ_s^m, $\mu_2 - \mu_s$ is fixed to 0.44, $\mathrm{I}_0 = 0.6$ and $b = 2/3$. The reduction of μ_s can be justified based on concentration profiles measurements by Sumer et al. (1996), Pugh and Wilson (1999) and Matoušek (2009). These authors report on values of the friction coefficient between 0.2 to 0.36 for the sheet layer thickness versus Shields number model to match the experimental values. Revil-Baudard et al. (2015) also mentioned a friction coefficient value as low as 0.2 in their experiments. Run RB3 is performed with these values (summarized in Table 2) and the results are shown in Fig. 2. The velocity profile is in better agreement with the experiment and the suspension is slightly overestimated, exhibiting a concentration shoulder on the mean concentration profile. Concerning Sumer et al. (1996) configurations, the velocity profiles predicted using the optimized rheological parameters (SUMA2/B2/C2) shown in Fig. 3 are in better agreement with the measurements, especially in the denser part of the flow. However, the velocity magnitude in the upper part of the profile is underestimated. This could be due to a lower value of the von Karman constant for these configurations. To conclude the discussion of this calibration/validation, the proposed model is able to reproduce almost quantitatively the experimental data for the depth profiles of average quantities. Nevertheless, some questions remain on the actual choice of the rheological parameters and on the von Karman constant

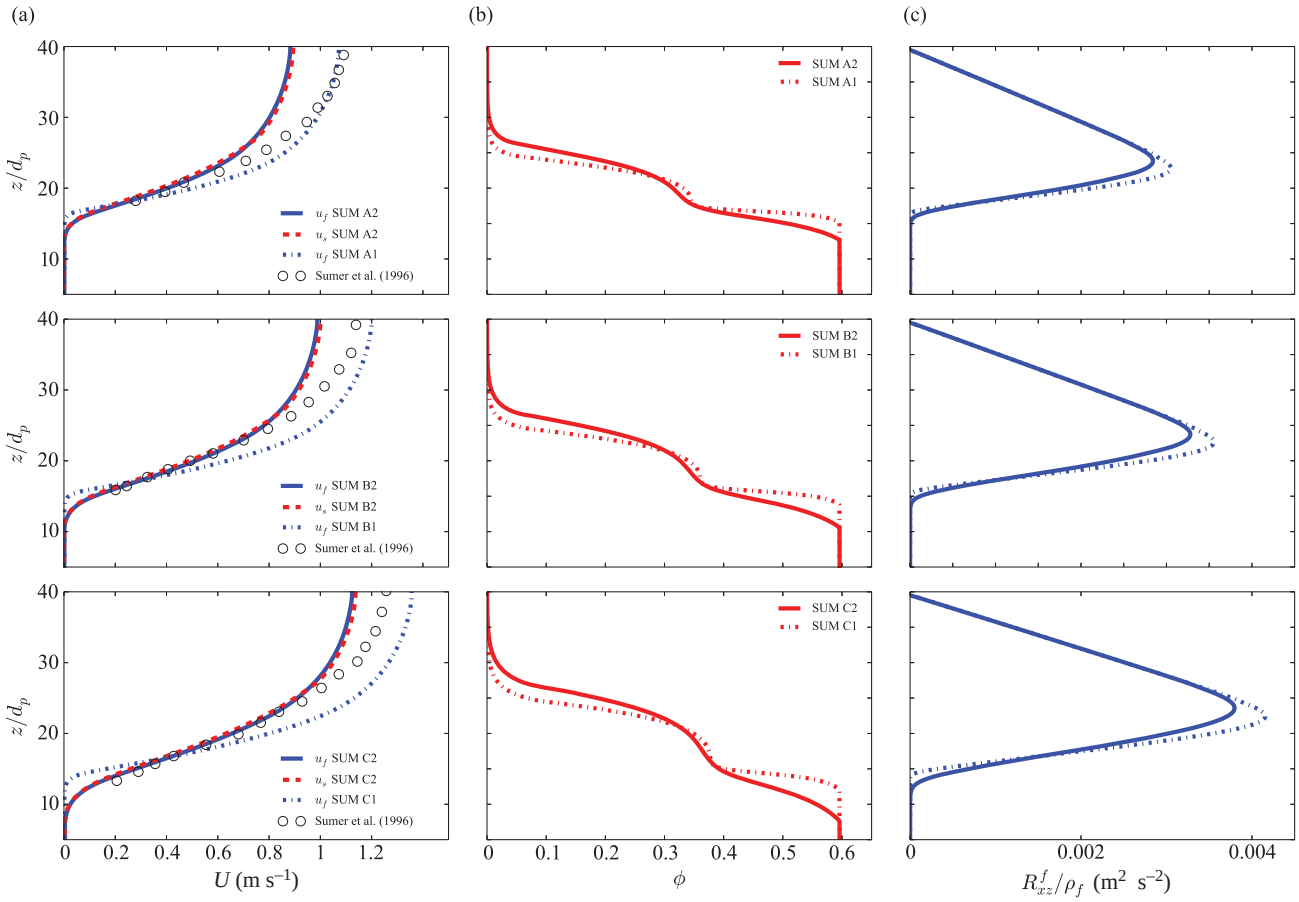

Figure 3 Comparison of numerical results with experimental data from Sumer et al. (1996) (symbols) in terms of fluid velocity profile (a), concentration profile (b) and Reynolds shear stress profile (c) for case SUM A1 (u_f : blue dash dotted lines) and SUM A2 (u_f : blue solid lines; u_s: red dashed lines) in the top panels, SUM B1 and SUM B2 in the middle panels and SUM C1 and SUM C2 in the bottom panels. The legend is the same for the cases B and C as for case A

value for sheet flow conditions. The model should be compared with detailed experiments for a wider range of flow conditions and sediment properties (density, size and shape). More sophisticated turbulence models, e.g. the $k-\varepsilon$ or $k-\omega$ models or turbulence resolving simulations (large eddy simulations), could help to improve our understanding of the complex interactions between the granular dynamics and the fluid turbulent boundary layer.

Beyond the validation on depth profiles, the model is further compared with experimental data and other model predictions for the dimensionless sediment transport rate $\overline{q_s} = q_s/\sqrt{(\rho_s/\rho_f - 1)g{d_p}^3}$ and the dimensionless sheet layer thickness $\overline{\delta_s} = \delta_s/d_p$ over a wide range of Shields numbers. Figure 4a shows the dimensionless sediment transport rate versus the Shields number for cases RB3, SUMA2/B2/C2 and four other simulations, with the same parameters as Sumer et al. (1996) cases but with different water depths corresponding to different Shields numbers. Overall the range of Shields numbers investigated is $\theta \in [0.44\text{–}3.3]$. The sediment transport rate per unit width is computed as: $q_s = \int_0^h u_s \phi \, \mathrm{d}z$ where the integral is performed over the entire domain, i.e. it corresponds to the total sediment transport rate including the contribution of the suspended load. The model predictions are compared with experimental data from the literature (Capart & Fraccarollo, 2011; Meyer-Peter & Muller, 1948; Nnadi & Wilson, 1992; Sumer et al., 1996; Wilson, 1966) and the model predictions from Capart and Fraccarollo (2011), Hsu et al. (2004), Wilson (1987) and Berzi and Fraccarollo (2013). The present results are in good agreement with experimental data from Nnadi and Wilson (1992) with sand and Bakelite particles and with two-phase numerical simulations from Hsu et al. (2004) and Berzi and Fraccarollo (2013) using two-phase flow model based on the kinetic theory of granular flows. The sediment transport rate predicted by the proposed two-phase flow model is slightly lower than the one predicted by Hsu et al. (2004), by a factor of two at most, and exhibit a power law relationship with the Shields number with an exponent of two (see the red dash-dotted line in the inset of panel (a) in log–log scales). It is remarkable that the proposed model gives almost identical results to the one obtained by the Berzi and Fraccarollo (2013) model based on the extended kinetic theory, on the exact same configurations. In the inset of Fig. 4a, it is observed that both models predict the

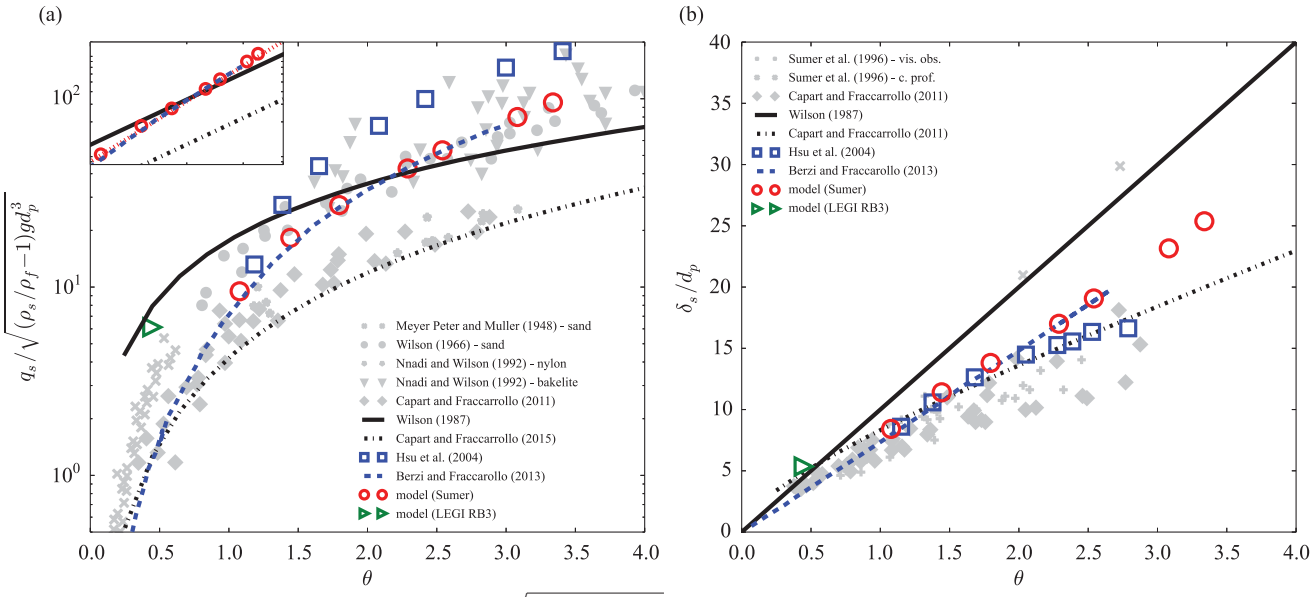

Figure 4 Dimensionless sediment transport rate $\overline{q_s} = q_s/\sqrt{(\rho_s/\rho_f - 1)gd_p^3}$: (a) dimensionless sheet layer thickness $\overline{\delta_s} = \delta_s/d_p$ (b) versus the Shields number θ predicted by the proposed two-phase flow model. °: Sumer et al. (1996) configurations ; ▷: Revil-Baudard et al. (2015) configuration; □: two-phase flow simulations from Hsu et al. (2004); × : Meyer-Peter and Muller (1948) data with sand; •: Wilson (1966) data with sand; ▼: (Nnadi and Wilson, 1992) data with nylon; ⋆: Nnadi and Wilson (1992) data with Bakelite; ◇: Capart and Fraccarollo (2011) data with PVC cylinders; +: Sumer et al. (1996) data with sand; ——: the Wilson (1987) fit $\overline{q_s} = 11.8\ \theta^{1.5}$ and $\overline{\delta_s} = 10\ \theta$; − − −: the Capart and Fraccarollo (2011) model $\overline{q_s} = 4.2\ \theta^{1.5}$ and $\overline{\delta_s} \propto \theta^{1.5}$ (see Eq. (7) in the original paper). The inset in panel (a) shows the dimensionless sediment transport rate versus the Shields number in log-log scales, the red dash-dotted line corresponds to a quadratic law

exact same power law exponent with an exponent of two, and not one and a half as suggested by most empirical formulas (e.g. Wilson, 1987).

Figure 4b shows the dependence of the sheet layer thickness on the Shields number. For the numerical simulation the sheet-layer thickness is defined as the vertical extent between the position at which the volume fraction is equal to 0.08, i.e. $\max(\{z|\phi \geq 0.08\})$ and the position at which the streamwise component of the particle phase velocity is lower than 0.02 m/s, i.e. $\min(\{z|u_s \geq 0.02\})$. These definitions are consistent with Hsu et al. (2004) and Revil-Baudard and Chauchat (2013) ones. The trend is linear with the Shields number and the results are in good agreement with Capart and Fraccarollo (2011) measurements based on concentration profile measurements and the authors' model. Again, the results from the Berzi and Fraccarollo (2013) model are almost identical to the proposed two-phase flow model predictions.

Figure 4a clearly illustrates the scatter in the data as well as in the model predictions. It is noteworthy that the experimental results reported in Capart and Fraccarollo (2011) with PVC particles and in Nnadi and Wilson (1992) with nylon particles correspond to lower sediment transport rate for a given Shields number. The suspended-load contribution could be responsible for the observed difference but no clear correlation has been observed between the sediment transport rate and the suspension number S (not shown here). Another argument could be the submergence, which is smaller in the experiments of Capart and Fraccarollo (2011) than in those of Sumer et al. (1996). The turbulent boundary layer and the suspension layer could be significantly affected in the experiments of Capart and Fraccarollo (2011). It could lead to a lower sediment transport rate and a thinner sheet layer. The mixing length model proposed by Berzi and Fraccarollo (2015), based on the same dataset, gives additional arguments for the influence of the small submergence. This reason could partly explain the discrepancies observed between the two experimental datasets, but this requires further investigation.

The fact that the proposed model gives very similar results to the Berzi and Fraccarollo (2013) model tends to demonstrate that the dense granular flow rheology $\mu(\mathrm{I})/\phi(\mathrm{I})$ can be used as an alternative approach to the kinetic theory to describe intergranular stresses in two-phase flow models for sheet flow applications. The great advantage of this rheological approach is that no additional transport equations have to be solved for the granular temperature, leading to simpler model equations. The main drawback is the number of empirical parameters that are required (μ_2, I_0 and b). Based on the careful calibration presented in this paper, the model can now be used to predict sheet flows with similar particles without further calibration. The main limitation of both approaches, kinetic theory and dense granular flow rheology, is still the lack of understanding of the complex interactions between the turbulence and the granular dynamic. High resolution experimental data on a wider range of flow conditions and particle properties together with turbulence resolving simulations are required to further improve our understanding of intergranular stress and turbulence models for sheet flow regime.

A potential issue has been raised by Barker, Schaeffer, Bohorquez, and Gray (2015), the $\mu(\mathrm{I})$ rheology is ill-posed for dry granular flows at very low and very high values of the inertial number I (for flow on an inclined plane). This result has been obtained without the volume fraction law $\phi(\mathrm{I})$ and according to the authors it is not clear whether the inclusion of an additional $\phi(\mathrm{I})$ dependence will be sufficient to prevent ill-posedness. In the meantime, two groups of researchers have been able, independently, to obtain numerical solutions of 2D and 3D granular flow problems using a regularized version of the $\mu(\mathrm{I})$ rheology (Chauchat & Médale, 2010, 2014; Lagrée, Staron, & Popinet, 2011; Staron, Lagrée, & Popinet, 2012, 2014) without observing the instabilities mentioned in Barker et al. (2015). Another argument against the ill-posedness issue is that in two-phase flow models for sediment transport the solid phase momentum equation in the dilute region of the flow, corresponding to high values of the inertial number, is tightly coupled with the fluid one and the ill-posedness of the granular rheology could be screened by the well-posed fluid flow problem. The potential ill-posedness of the $\mu(\mathrm{I})$ rheology has to be kept in mind when developing a multi-dimensional numerical model.

4 Conclusion

In this paper, an extension of the two-phase flow model proposed in Revil-Baudard and Chauchat (2013) has been presented. The main improvement concerns the single layer formulation adopted herein, i.e. the model is based on the same set of mass and momentum conservation equations from the fixed sediment bed up to the free surface. The mixing length formulation has been improved and validated on experimental measurements under sheet-flow conditions and can now be used to describe the turbulent boundary layer above mobile beds. A drift velocity has been introduced to represent the turbulent dispersion terms that allow recovery of the Rouse profile. The model is shown to reproduce quite well the experimental data from Revil-Baudard et al. (2015) and Sumer et al. (1996), provided that the granular rheology parameters are modified compared with classical values for glass spheres in air. The comparison with other experimental data and models for the sediment transport rate and the sheet layer thickness are in good agreement, showing that the model can be used as a predictive tool. The only parameter that remains to be adjusted is the static friction coefficient, μ_s; the others can be calculated based on the method proposed in this paper: $\mu_2 = \mu_s + 0.44$, $\mathrm{I}_0 = 0.6$ and $b = 2/3$. For the mixing length, the dependency of the von Karman constant with the Shields and suspension numbers is still unclear and a parametrization based on experiments remains to be established. For the Schmidt number, the proposition of Van Rijn (1984) can be used even if, again, new high resolution measurements could help to improve this parametrization. The most important result of the present paper is probably the very good agreement between the proposed dense granular flow based model and the extended kinetic theory based model from Berzi and Fraccarollo (2013), demonstrating that the dense granular flow rheology can be used in two-phase flow sediment transport models as an alternative to the kinetic theory.

In terms of perspectives, the proposed model has been used in conjunction with fluid-discrete element method simulation of bed-load transport (Maurin, Chauchat, & Frey, 2016) to better characterize the dense granular flow rheology for application to sediment transport. In the meantime, the proposed model will be implemented in sedFOAM, a 3D open source two-phase sediment transport model based on openFOAM (Cheng, Hsu, & Calantoni, 2017), that will open new perspectives in terms of applications of the model on more complex geometries and flow conditions.

Acknowledgements

The author thanks Thibaud Revil-Baudard, David Hurther, Raphael Maurin, Philippe Frey and Tian-Jian Hsu for fruitful discussions on experimental and modelling aspects of sheet-flows and granular flow rheology. The author would also like to acknowledge the support from the program on Fluid-Mediated Particle Transport in Geophysical Flows at the Kavli Institute for Theoretical Physics, Santa Barbara, USA. The laboratory LEGI is part of the LabEx Tec 21 (Investissements dAvenir - grant agreement nANR-11-LABX-0030).

Funding

This work was supported by the Région Rhones-Alpes (COOPERA project and Explora Pro grant) and the French national programme EC2CO-LEFE MODSED. 10.13039/50110 0004617 Institut National des Sciences de l'Univers, Centre National de la Recherche Scientifique.

Appendix 1. Recovering the Rouse profile

In this appendix, we will detail how the so-called Rouse profile (Rouse, 1937) and the two-phase equations presented in Section 2 can be reconciled. A similar demonstration can be found in Greimann, Muste, and Holly (1999).

The Rouse profile corresponds to the balance between the settling flux $w\phi$ and the upward turbulent dispersion term $\overline{w_s'\phi'}$ and leads to the following equation:

$$w\phi + \overline{w_s'\phi'} = 0 \tag{A1}$$

where w represents the settling velocity of the sediment. The overline corresponds to the time averaging in the Reynolds averaging process. Following Rouse (1937), the turbulent dispersion

flux can be modelled as a diffusion process according to:

$$\overline{w_s'\phi'} = -\frac{\nu_f^t}{\sigma_s}\frac{\partial \phi}{\partial z} \tag{A2}$$

where ν_f^t represents the eddy viscosity and σ_s the Schmidt number. The Rouse profile is obtained by solving analytically the first order ordinary differential equation in ϕ:

$$\frac{\partial \phi}{\partial z} + \frac{w\sigma_s}{\nu_f^t}\phi = 0 \tag{A3}$$

in which ν_f^t follows a Prandtl-like relationship:

$$\nu_f^t = u_*^2 \kappa z \left(1 - \frac{z}{h}\right) \tag{A4}$$

where u_* is the bed friction velocity, κ the von Karman constant, and h the water depth. The solution of Eq. (A3) with eddy viscosity given by Eq. (A4) gives the so-called Rouse profile:

$$\frac{\phi}{\phi^{ref}} = \left(\frac{\frac{h}{z} - 1}{\frac{h}{z^{ref}} - 1}\right)^{w\sigma_s/(\kappa u_*^2)} \tag{A5}$$

We now switch to the two-phase equations: at steady-state the vertical velocity of both phases vanishes (i.e. $w_s = w_f = 0$), so the vertical component of the momentum Eqs (9) and (10) simplifies to:

$$0 = -\epsilon\frac{\partial p_f}{\partial z} - \epsilon\rho_f g\cos(\beta) - \frac{\phi\rho_s}{\tau_{fs}}w_d \tag{A6}$$

$$0 = -\frac{\partial p_s}{\partial z} - \phi\frac{\partial p_f}{\partial z} - \phi\rho_s g\cos(\beta) + \frac{\phi\rho_s}{\tau_{fs}}w_d \tag{A7}$$

The mixture momentum equation is obtained by adding Eqs (A6) and (A7):

$$0 = -\frac{\partial p_s}{\partial z} - \frac{\partial p_f}{\partial z} - ((1-\phi)\rho_f + \phi\rho_s)g\cos(\beta) \tag{A8}$$

For solid phase volume fraction lower than a critical value ϕ^c the particulate pressure vanishes ($p_s = 0$), meaning that no normal stress develops between the particles. They have no intrinsic resistance to compression. The vertical fluid pressure gradient balances the mixture weight:

$$\frac{\partial p_f}{\partial z} = -((1-\phi)\rho_f + \phi\rho_s)g\cos(\beta) \tag{A9}$$

Introducing this relationship in Eq. (A7) leads to the equilibrium between gravity and vertical dispersion effect:

$$0 = -(1-\phi)\left(1 - \frac{\rho_f}{\rho_s}\right)g\cos(\beta) + \frac{w_d}{\tau_{fs}} \tag{A10}$$

In order to identify this equilibrium with the Rouse mass balance equation, we have to express the settling flux in absence of turbulence. It is given by the two-phase equation by neglecting the drift velocity; this is equivalent to Eq. (A10) with $-w_s$ instead of w_d:

$$\phi w_s + \phi(1-\phi)\left(1 - \frac{\rho_f}{\rho_s}\right)g\cos(\beta) \quad \tau_{fs} = 0 \tag{A11}$$

which leads to:

$$\frac{w_s}{\tau_{fs}} = -(1-\phi)\left(1 - \frac{\rho_f}{\rho_s}\right)g\cos(\beta) \tag{A12}$$

Greimann et al. (1999) obtained the same result by using the definition of the particle relaxation time.

By identifying the right hand side of Eq. (A12) with Eq. (A10) and using Eq. (A1) we obtain that:

$$\overline{w_s'\phi'} = \phi w_d \tag{A13}$$

Therefore, in order to recover the Rouse profile in the two-phase framework the following relationship for the drift velocity must be used:

$$w_d = -\frac{\nu_f^t}{\sigma_s\phi}\frac{\partial \phi}{\partial z} \tag{A14}$$

This is what is classically done in two-phase sediment transport models (Chauchat & Guillou, 2008; Hsu et al., 2004).

Notation

b	=	parameter of the dilatancy law (–)
C_D	=	drag coefficient (–)
d_p	=	particle diameter (m)
$\tilde{d}_p$	=	particle diameter corrected for shape effect (m)
$\boldsymbol{f_D}$	=	drag vector force on a particle (kg m^{-2} s^{-2})
$\boldsymbol{g}$	=	gravity acceleration vector (m s^{-2})
I	=	inertial number (–)
I_0	=	empirical parameter of the granular rheology (–)
l_m	=	mixing length (m)
n	=	number density of particle (–)
n_{lm}	=	mixing length exponent (–)
n_{RZ}	=	Richardson and Zaki's exponent (–)
p_k	=	pressure of phase k (Pa)
p_s^c	=	particle pressure originating from permanent contact (Pa)
p_s^s	=	particle pressure originating from shear induced mechanisms (Pa)
q_s	=	sediment transport rate per unit width (m^2 s^{-1})
$\overline{q_s}$	=	dimensionless sediment transport rate per unit width (–)
$\mathbf{R_f}$	=	Reynolds stress tensor (Pa)
R_{xz}^f	=	xz component of the Reynolds shear stress (Pa)
R_p	=	particulate Reynolds number (–)
S	=	suspension number (–)

S_f = friction slope (–)
u_* = bed friction velocity ($\mathrm{m\,s^{-1}}$)
$\boldsymbol{u_d}$ = drift velocity vector ($\mathrm{m\,s^{-1}}$)
$\boldsymbol{u}_k$ = velocity vector of phase k ($\mathrm{m\,s^{-1}}$)
u_k = streamwise velocity component of phase k ($\mathrm{m\,s^{-1}}$)
U = streamwise volume averaged mixture velocity ($\mathrm{m\,s^{-1}}$)
w_k = wall normal velocity component of phase k ($\mathrm{m\,s^{-1}}$)
w = settling velocity ($\mathrm{m\,s^{-1}}$)
z_d = zero plane bed (m)
z_{int} = initial bed interface elevation (m)
β = channel slope (rad)
δ_s = sheet layer thickness (m)
$\overline{\delta_s}$ = dimensionless sheet layer thickness (–)
ϵ = Solid phase volume fraction (–)
ζ = particle pressure exponent (–)
η_f = fluid dynamical viscosity ($\mathrm{kg\,m^{-1}\,s^{-1}}$)
η_{mix} = mixture dynamical viscosity ($\mathrm{kg\,m^{-1}\,s^{-1}}$)
η_s = solid phase viscosity ($\mathrm{kg\,m^{-1}\,s^{-1}}$)
η_t = eddy viscosity ($\mathrm{kg\,m^{-1}\,s^{-1}}$)
θ = Shields number (–)
κ = von Karman constant (–)
λ = regularization parameter ($\mathrm{s^{-1}}$)
μ = friction coefficient (–)
μ_s = static friction coefficient for the rheology (–)
μ_s^m = measured static friction coefficient (–)
μ_2 = dynamic friction coefficient for the rheology (–)
ν_f = fluid kinematic viscosity ($\mathrm{m^2\,s^{-1}}$)
Π_0 = particle pressure modulus (Pa)
ρ_k = density of phase k ($\mathrm{kg\,m^{-3}}$)
σ_{s} = Schmidt number (–)
$\boldsymbol{\tau}_k$ = stress tensor of phase k (Pa)
τ_{xz}^k = xz stress component of phase k (Pa)
τ_{fs} = particle relaxation time (s)
ϕ = Solid phase volume fraction (–)
ϕ^0 = initial solid volume fraction (–)
$\phi^{\max}$ = maximum packing volume fraction (–)
ψ = shape factor (–)

References

Aussillous, P., Chauchat, J., Pailha, M., Médale, M., & Guazzelli, E. (2013). Investigation of the mobile granular layer in bedload transport by laminar shearing flows. *Journal of Fluid Mechanics*, *736*, 594–615.

Bagnold, R. A. (1954). Experiments on a gravity-free dispersion of large solid spheres in a newtonian fluid under shear. *Philosophical Transactions of the Royal Society of London, Series A: Mathematical, Physical and Engineering Sciences*, *225*, 49–63.

Bagnold, R. A. (1956). The flow of cohesionless grains in fluids. *Philosophical Transactions of the Royal Society of London, Series A: Mathematical, Physical and Engineering Sciences*, *249*, 235–297.

Barker, T., Schaeffer, D. G., Bohorquez, P., & Gray, J. M. N. T. (2015). Well-posed and ill-posed behaviour of the rheology for granular flow. *Journal of Fluid Mechanics*, *779*, 794–818.

Berzi, D. (2011). Analytical solution of collisional sheet flows. *Journal of Hydraulic Engineering*, *137*(10), 1200–1207.

Berzi, D., & Fraccarollo, L. (2013). Inclined, collisional sediment transport. *Physics of Fluids*, *25*(10), 106601-1–106601-11.

Berzi, D., & Fraccarollo, L. (2015). Turbulence locality and Granularlike fluid shear viscosity in collisional suspensions. *Physical Review Letters*, *115*, 194501. doi:10.1103/PhysRevLett.115.194501

Berzi, D., & Fraccarollo, L. (2016). Intense sediment transport: Collisional to turbulent suspension. *Physics of Fluids*, *28*(2), 023302-1–023302-12.

Bouvard, M., & Petkovic, S. (1985). Vertical dispersion of spherical, heavy particles in turbulent open channel flow. *Journal of Hydraulic Research*, *23*(1), 5–20.

Boyer, F. M. C., Guazzelli, E., & Pouliquen, O. (2011). Unifying suspension and granular rheology. *Physical Review Letters*, *107*, 188301. doi:10.1103/PhysRevLett.107.188301

Capart, H., & Fraccarollo, L. (2011). Transport layer structure in intense bed-load. *Geophysical Research Letters*, *38*(20). doi:10.1029/2011GL049408

Cassar, C., Nicolas, M., & Pouliquen, O. (2005). Submarine granular flows down inclined planes. *Physics of Fluids*, *17*(10), 103301.

Chauchat, J., & Guillou, S. (2008). On turbulence closures for two-phase sediment-laden flows models. *Journal Geophysical Research-Oceans*, *113*, 20.

Chauchat, J., Guillou, S., Bang, D. P. V., & Nguyen, K. D. (2013). Modelling sedimentation–consolidation in the framework of a one-dimensional two-phase flow model. *Journal of Hydraulic Research*, *51*(3), 293–305.

Chauchat, J., & Médale, M. (2010). A 3D numerical model for incompressible two-phase flow of a granular bed submitted to a laminar shearing flow. *Computer Methods in Applied Mechanics and Engineering*, *199*, 439–449.

Chauchat, J., & Médale, M. (2014). A three-dimensional numerical model for dense granular flows based on the rheology. *Journal of Computational Physics*, *256*(0), 696–712. Retrieved from http://www.sciencedirect.com/science/article/pii/S0021999113006098

Cheng, Z., Hsu, T.-J., & Calantoni, J. (2017). SedFoam: A multi-dimensional Eulerian two-phase model for sediment transport and its application to momentary bed failure. *Coastal Engineering*, *119*, 32–50. doi:10.1016/j.coastaleng.2016.08.007.

Chiodi, F., Claudin, P., & Andreotti, B. (2014). A two-phase flow model of sediment transport: Transition from bedload to suspended load. *Journal of Fluid Mechanics*, *755*, 561–581.

Chorin, A. J. (1968). Numerical simulation of Navier-Stokes equations. *Mathematics of Computation*, *22*, 745–762.

Courrech du Pont, S., Gondret, P., Perrin, B., & Rabaud, M. (2003). Granular avalanches in fluids. *Physical Review Letters*, *90*, 044301. doi:10.1103/PhysRevLett.90.044301

Daniel, S. (1965). *Flow of suspension in a rectangular channel* (Unpublished doctoral dissertation).

Dong, P., & Zhang, K. (1999). Two-phase flow modelling of sediment motions in oscillatory sheet flow. *Coastal Engineering*, *36*(2), 87–109. Retrieved from http://www.sciencedirect.com/science/article/B6VCX-3W19GCV-1/2/ac8de4577f0ef05e935c824062632329

Einstein, H.-A. (1950). *The bed load function for sedimentation in open channel channel flows* (Tech. Rep. No. 1026). U.S. Department of Agriculture.

Forterre, Y., & Pouliquen, O. (2008). Flows of dense granular media. *Annual Review of Fluid Mechanics*, *40*, 1–24. Retrieved from http://link.aip.org/link/?PHF/17/103301/1

GDRmidi. (2004). On dense granular flows. *The European Physical Journal E*, *14*, 341–365.

Greimann, B. P., Muste, M., & Holly, F. M. (1999). Two-phase formulation of suspended sediment transport. *Journal of Hydraulic Research*, *37*, 479–500.

Hanes, D. M., & Bowen, A. J. (1985). A granular-fluid model for steady intense bed-load transport. *Journal of Geophysical Research*, *90*, 9149–9158.

Hsu, T.-J., Jenkins, J. T., & Liu, P. L-F. (2004). On two-phase sediment transport: Sheet flow of massive particles. *Proceedings of the Royal Society of London A: Mathematical, Physical and Engineering Sciences*, *460*(2048), 2223–2250. Retrieved from http://rspa.royalsocietypublishing.org/content/460/2048/2223

Hurther, D., Thorne, P. D., Bricault, M., Lemmin, U., & Barnoud, J.-M. (2011). A multi-frequency Acoustic Concentration and Velocity Profiler (ACVP) for boundary layer measurements of fine-scale flow and sediment transport processes. *Coastal Engineering*, *58*, 594–605. Retrieved from http://www.sciencedirect.com/science/article/pii/S03783839 1100007X

Jackson, R. (1997). Locally averaged equations of motion for a mixture of identical spherical particles and a Newtonian fluid. *Chemical Engineering Science*, *52*, 2457–2469.

Jackson, R. (2000). *The dynamics of fluidized particles*. Cambridge: Cambridge University Press.

Jenkins, J. T., & Hanes, D. M. (1998). Collisional sheet flows of sediment driven by a turbulent fluid. *Journal of Fluid Mechanics*, *370*(1), 29–52.

Johnson, P. C., & Jackson, R. (1987). Frictional-collisional constitutive relations for granular materials, with application to plane shearing. *Journal of Fluid Mechanics*, *176*, 67–93.

Jop, P., Forterre, Y., & Pouliquen, O. (2006). A constitutive law for dense granular flows. *Nature*, *441*, 727–730. doi:10.1038/nature04801

Lagrée, P.-Y., Staron, L., & Popinet, S. (2011). The granular column collapse as a continuum: Validity of a two-dimensional Navier–Stokes model with a î(I)-rheology. *Journal of Fluid Mechanics*, *686*, 378–408. doi:10.1017/jfm.2011.335

Li, L., & Sawamoto, M. (1995). Multi-phase model on sediment transport in sheet-flow regime under oscillatory flow. *Coastal Engineering Japan*, *38*, 157–178.

Matoušek, V. (2009). Concentration profiles and solids transport above stationary deposit in enclosed conduit. *Journal of Hydraulic Engineering*, *135*(12), 1101–1106.

Maurin, R., Chauchat, J., & Frey, P. (2016). Dense granular flow rheology in turbulent bedload transport. *Journal of Fluid Mechanics*, *804*, 490–512. Retrieved from https://www.cambridge.org/core/article/dense-granular-flow-rheology-in-turbulent-bedload-transport/154F85CA45BEE6EC15D0CBF869670597

Meyer-Peter, E., & Muller, R. (1948). *Formulas for bed-load transport*. 2nd meeting of the International Association of Hydraulic and Structural Research, Stockholm (pp. 34–64).

Muste, M., & Patel, V. C. (1997). Velocity profiles for particles and liquid in open-channel flow with suspensded sediment. *Journal of Hydraulic Engineering*, *123*, 742–751.

Nnadi, F. N., & Wilson, K. C. (1992). Motion of contact-load particles at high shear stress. *Journal of Hydraulic Engineering*, *118*(12), 1670–1684. Retrieved from http://link.aip.org/link/?QHY/118/1670/1

Ouriemi, M., Aussillous, P., & Guazzelli, E. (2009). Sediment dynamics. Part I: Bed-load transport by shearing flows. *Journal of Fluid Mechanics*, *636*, 295–319.

Pugh, F. J., & Wilson, K. C. (1999). Velocity and concentration distributions in sheet flow above plane beds. *Journal of Hydraulic Engineering*, *125*(2), 117–125.

Revil-Baudard, T., & Chauchat, J. (2013). A two-phase model for sheet flow regime based on dense granular flow rheology. *Journal of Geophysical Research: Oceans*, *118*(2), 619–634. doi:10.1029/2012JC008306

Revil-Baudard, T., Chauchat, J., Hurther, D., & Barraud, P.-A. (2015). Investigation of sheet-flow processes based on novel acoustic high-resolution velocity and concentration measurements. *Journal of Fluid Mechanics*, *767*, 1–30.

Richardson, J. F., & Zaki, W. N. (1954). Sedimentation and fluidization: Part I. *Transactions of the Institution of Chemical Engineers*, *32*, 35–53.

Rouse, H. (1937). Modern conceptions of the mechanics of turbulence. *Transactions of the American Society of Civil Engineers*, *102*, 463–505.

Schiller, L., & Naumann, A. (1933). Uber die Grundlegenden Berechungen bei der Schwerkraftaufbereitung. *Zeitschrift des Vereins Deutscher Ingenieure*, *77*, 318–320.

Simonin, O., & Viollet, P. L. (1990). *Numerical study on phase dispersion mechanisms in turbulent bubbly flows*.

Proceedings 5th workshop on two-phase flow predictions, Taipei, Taiwan (pp. 156–166).

Spinewine, B., Capart, H., Fraccarollo, L., & Larcher, M. (2011). Laser stripe measurements of near-wall solid fraction in channel flows of liquid-granular mixtures. *Experiments in Fluids*, *50*, 1507–1525. doi:10.1007/s00348-010-1009-7

Staron, L., Lagrée, P.-Y., & Popinet, S. (2012). The granular silo as a continuum plastic flow: The hour-glass vs the clepsydra. *Physics of Fluids*, *24*(10), 103301. Retrieved from http://link.aip.org/link/?PHF/24/103301/1

Staron, L., Lagrée, P. Y., & Popinet, S. (2014). Continuum simulation of the discharge of the granular silo. *European Physical Journal E: Soft Matter*, *37*(1), 5. doi:10.1140/epje/i2014-14005-6

Sumer, B. M., Kozakiewicz, A., Fredsoe, J., & Deigaard, R. (1996). Velocity and concentration profiles in sheet-flow layer of movable bed. *Journal of Hydraulic Engineering*, *122*(10), 549–558. Retrieved from http://link.aip.org/link/?QHY/122/549/1

Temam, R. (1969). Sur l'approximation des équations de Navier-Stokes par la méthode des pas fractionnaires (ii). *Archive for Rational Mechanics and Analysis*, *26*, 367–380.

Van Rijn, L. C. (1984). Sediment pickup functions. *Journal of Hydraulic Engineering*, *110*, 1494–1502.

Wilson, K. C. (1966). Bed-load transport at high shear stress. *Journal of Hydraulics Division, ASCE*, *92*(HY6), 49–59.

Wilson, K. C. (1987). Analysis of bed-load motion at high shear stress. *Journal of Hydraulic Engineering*, *113*, 97–103.

Yalin, M. S. (1977). *Mechanics of sediment transport* (2nd ed.). Ontario: Pergamon Press.